

Preparation and sensing properties of mesoporous ZnO–rGO composites based on in situ hydrothermal synthesis

Yue Shen¹ · Sicheng Luo¹ · Zhongrui Wu¹ · Meng Cao¹ · Feng Gu¹ · Linjun Wang¹

Received: 22 February 2016 / Accepted: 19 July 2016 / Published online: 30 July 2016
© Springer Science+Business Media New York 2016

Abstract Zinc oxide/graphene (ZnO–rGO, rGO is short for reduced graphene) nano-composites were prepared by in situ reduction of zinc acetate((CH₃COO)₂Zn·2H₂O) and graphene oxide (GO) with a simple hydrothermal process assisted with Pluronic P123 triblock copolymer. Adsorbents of the gas sensing devices based on nanocomposite were prepared by coating method. The films have mesoporous structures and contain nano-crystalline phase, as evidenced from N₂ adsorption–desorption isotherms, X-ray diffraction and high resolution scanning electron microscopy. Gas sensing properties of pure ZnO and ZnO–rGO nano-composites were investigated in the temperature range of 100–300 °C. Compared with ZnO, ZnO–rGO nano-composite samples have enhanced hydrogen sulfide sensing properties. When the concentration of hydrogen sulfide reached 50 ppm, sensitivity of ZnO–rGO (5 wt%) reached 55.91 at 160 °C, which was about dozens of times higher than that of pure ZnO.

1 Introduction

As n-type functional semiconductor, ZnO has attracted wide attention in gas-sensing applications to detect toxic and volatile gases such as ethanol, acetone, ammonia, nitrogen dioxide and hydrogen sulfide in recent years, due to its excellent conductive electron mobility and good adsorption characteristics under the normal working conditions of the sensors [1–9]. But sensors based on

intrinsic ZnO usually have high working temperatures (400–500 °C). Doping other materials into ZnO to obtain composites may be a proper method to reduce the operating temperature of gas sensors [10–14]. Graphene oxide (GO) has been widely studied as an adsorbent since it contains various oxygen functional groups and has large BET specific surface area [15–17]. The oxygen functional groups in GO can anchor positively charged metal ions (i.e. Zn²⁺ or Cu⁺) by hydrogen bonds [15, 18–21]. Therefore, ZnO–rGO nano-composites can be used to detect acid gas (i.e. H₂S, SO₂, NO₂ or NO). Several groups have successfully fabricated composites of ZnO and rGO by UV-light irradiation, microwave irradiation and simple solvo-thermal methods, and used for gas detection [22–24]. ZnO–rGO composites have been synthesized by microwave irradiation method and used for hydrogen sulfide detection at 300 °C in Yi's group [25]. Three-dimensional graphene aerogel–ZnO spheres composites were prepared in Zhang's group via simple solvothermal method [26]. However, many of these devices have to work at about 300 °C. Few studies have focused on gas detection properties of ZnO–rGO nano-composite at low temperature even at room temperature. In this paper, mesoporous ZnO–rGO was synthesized by a green and simple hydrothermal method assisted with Pluronic P123 triblock copolymer, and it was used to fabricate gas sensors, which exhibited excellent response to hydrogen sulfide at low temperature.

2 Experimental

In this paper, Pluronic P123 triblock copolymer (poly(ethylene glycol)-block-poly(propylene glycol)-block-poly(ethylene glycol)) with a molar weight of 5800 was purchased from Sigma-Aldrich, and all other chemicals

✉ Yue Shen
yueshen@shu.edu.cn

¹ School of Materials Science and Engineering, Shanghai University, Shanghai 200072, China

were analytical grade and purchased from Sinopharm Chemical Reagents.

2.1 Synthesis of graphene oxide (GO)

Graphene oxide was synthesized by a modified Hummer's method [27, 28]. In detail, concentrated H_2SO_4 (360 mL), H_3PO_4 (40 mL) and graphene (3 g) were mixed together and kept ultrasonic scattering and stirring for 5 min. Then 20 g potassium permanganate was added into the solution slowly under ultrasonication. Following water bath for 12 h, ice block was put in the mixture with continuous stirring until temperature of the solution cooled down to room temperature. At last, H_2O_2 (30 %) was dropped into the solution until there was no more gas generation. The suspension in the solution was washed and centrifuged repeatedly with deionized water three times. Then the product was washed with ethanol and dried for precursor.

2.2 Synthesis of gas sensing materials

ZnO-rGO and pure ZnO were both prepared by a facile and simple hydrothermal method assisted with P123. For pure ZnO, 0.548 g P123, 1.1 g $\text{Zn}(\text{AC})_2 \cdot 2\text{H}_2\text{O}$ and 1.5 g urea were mixed in 100 mL deionized water, then the solution were stirred until it was clear. one mL hydrazine hydrate was added into the mixture with a stirring procedure for 2 h, then was transferred to a Teflon reactor, which was maintained at 90 °C for 24 h. The precipitation in the bottom of Teflon reactor was separated by filtration, and then rinsed with ethanol and deionized water for several times and dried at 90 °C overnight to obtain ZnO powders. ZnO powders were annealed at 350 °C in nitrogen condition for 4 h with the heating rate of 2 °C per minute. The ZnO obtained was noted as Z-0. For ZnO-rGO nanocomposite, the synthesis procedure was basically the same as that of pure ZnO, except that we added a certain proportion of GO precursor into deionized water after P123, $\text{Zn}(\text{AC})_2 \cdot 2\text{H}_2\text{O}$ and urea were added. The ratio of GO in precursor solution were determined as 0.5, 1, 2, 4, 5 and 10 wt%. These samples were signed as Z-0.5, Z-1, Z-2, Z-4, Z-5 and Z-10.

2.3 Fabrication of gas sensing devices

0.1 g required gas sensing materials was added into the agate mortar and ground for 15 min. Then, appropriate amount of Ethyl cellulose dissolved in ethanol (EC) were added to the mixture and grinded for 1 h. After that, the gas sensing film was fabricated on the prepared ceramic tubes with gold electrodes connected to both sides (made by Winsen tech) by drop-coating method and irradiated under infrared lamp for 15 min, then dried at 60 °C for 12 h. At

last, the ceramic tubes were annealed at 500 °C for 1 h with the heating rate of 5 °C per minute. The prepared ceramic tubes with gas sensing layer on them were welded to plastic bases with six pins for obtaining the complete devices. The structure of device was shown in Fig. 1.

2.4 Characterization of samples and devices

N_2 adsorption–desorption isotherms were tested in gas static adsorption instrument (JW-BK122F, JWGB), which used nitrogen as the adsorbate. ZnO-rGO composites were characterized by an X-ray diffractometer (RigakuD/MAX-2200, Tokyo) with Cu α radiation ($\lambda = 1.54 \text{ \AA}$), operated at 40 kV and 250 mA, the data were collected at a scanning rate of 0.1 deg/s for 2θ value in the range of 20–80°. Raman spectra were conducted under room temperature by JY Raman spectrometer (JY-HR800) equipped with a 514 nm He-Cd laser. An FEI Sirion 200 scanning electron microscope (SEM) was used to observe the surface of gas sensing layers. Gas sensing properties were measured on Gas-Sensitive Testing System (WS-30A, Winsen, China).

3 Results and discussion

3.1 Analysis of sensing materials

XRD patterns of GO, rGO and ZnO-rGO are tested and shown in Figs. 2 and 3. It can be found that GO have special 2θ peak at 9.7° in Fig. 2a, corresponding to the (001) reflection. The characteristic peak at 25.22° in Fig. 2b responded to (002) reflection of rGO. According to Fig. 3, all of the ZnO-rGO samples were crystallized well and shown obvious diffraction peaks of wurtzite ZnO, and peaks at 31.77°, 34.42°, 36.25°, 47.54°, 56.60°, 62.86°, 67.96°, 69.10°, 72.56° and 76.95° were indexed as (100), (002), (101), (102), (110), (103), (200), (112), (201), (004) and (202) planes of ZnO (according to ICDD card No. 36-1451). It is known that the characteristic tiny reflection

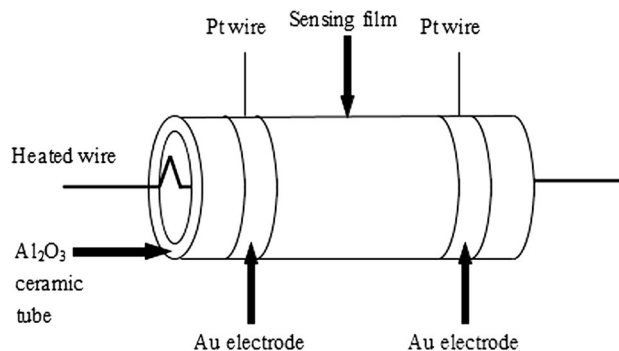


Fig. 1 Structure of the gas sensor

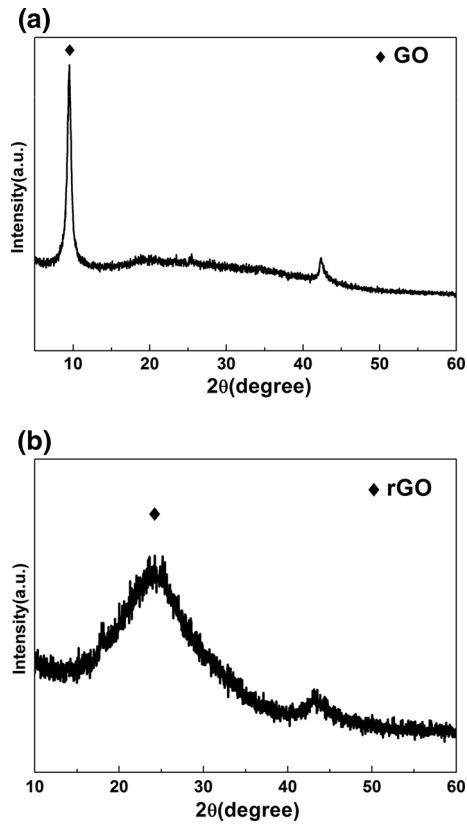


Fig. 2 XRD patterns of graphene oxide (GO) and reduced graphene oxide (rGO)

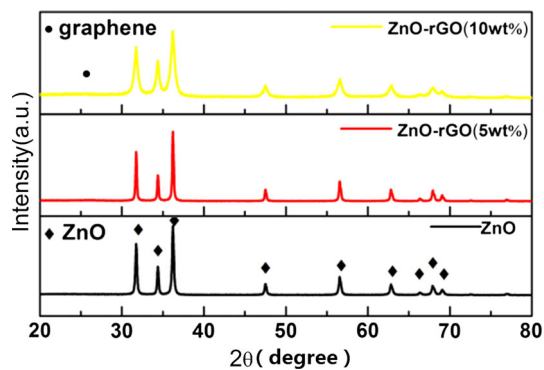


Fig. 3 XRD patterns of ZnO and ZnO-rGO nanocomposite

peak of graphene (002) appears at about $2\theta = 25.22^\circ$, but the reflection of rGO was not obvious in the XRD patterns of rGO-ZnO composites, which was attributed to the regular stack of rGO sheets were homogeneously dispersed and coated with ZnO. As shown in Fig. 3, full width at half maximum (FWHM) of XRD patterns of samples were almost the same as the doping ratio of rGO increased when doping ratio was smaller than 5 wt%, which indicated that doping proper amount of rGO into ZnO had tiny effect on the structure and property of ZnO crystal. As shown in

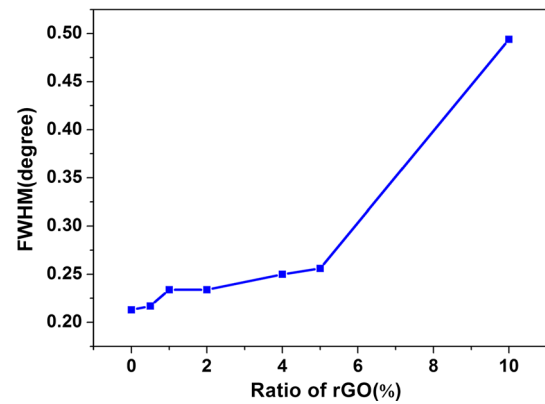


Fig. 4 Full width at half maximum of samples made by ZnO-rGO composites

Fig. 4, FWHM of sample Z-10 apparently became much wider (0.494°) than that of others (0.213° , 0.217° , 0.234° , 0.234° , 0.250° , 0.256°), which proved that grain size of sample Z-10 was much smaller than that of other samples according to Debye-Scherrer equation.

Raman spectra of ZnO-rGO and GO were shown in Fig. 5. It is clear that GO exhibits two main intrinsic peaks:

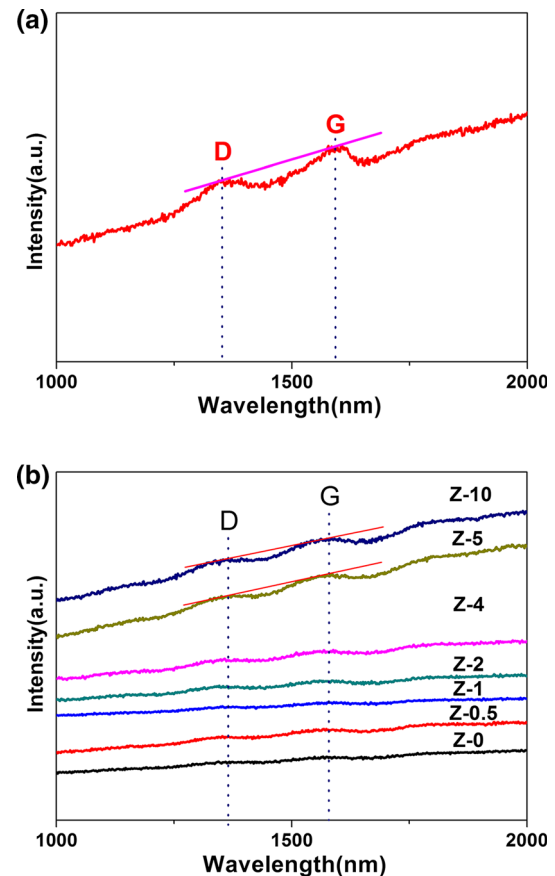


Fig. 5 Raman spectra of a graphene oxide, b ZnO and ZnO-rGO

the D band (at 1366 cm^{-1}), arising from a breathing mode of k-point photons of A_{1g} symmetry; and the G band (at 1577 cm^{-1}) originating from the first-order scattering of E_{2g} phonon of sp^2 carbon atoms [29]. As to ZnO–rGO in Fig. 5b, two prominent peaks of rGO still exist and appear at around 1360 and 1580 cm^{-1} . Notably, there is an increase in I_D/I_G (intensity ratio of D and G line) of ZnO–rGO (5 wt%) (0.92) compared with that of GO (0.84), suggesting a decrease of the average size of sp^2 domains upon the hydrothermal reduction and the occurrence of GO reduction [27].

Figure 6 exhibits FE-SEM images of surfaces of all the gas sensing layers. It was found that the size of particles became smaller and began to accumulate around graphene sheets as the ratio of rGO in ZnO–rGO composites arised. Figure 6a–c are the SEM images of gas sensors made by ZnO, ZnO–rGO (0.5 wt%) and ZnO–rGO (1 wt%), and the size of particles were about 1–2 μm . According to the inset images in Fig. 6d–g, the size of nanoparticles are about 200–500 nm.

The results of N_2 adsorption–desorption test of the ZnO and Zn–rGO powders were shown in Fig. 7. According to hysteresis loop between the adsorption and desorption curves and the change rules in Fig. 7, it can be concluded that mesoporous structure were presented in all of the samples, which were probably attributed to the adding of pore making agent P123 in hydrothermal process. The adsorption and desorption curves in Fig. 7a–e belongs to IV-type, which means the sample Z-0, Z-0.5, Z-1, Z-2 and Z-4 has mesoporous structure. But the curve in Fig. 7f changes more and like II-type, still there has an obvious hysteresis loop between the adsorption and desorption curve, which means the sample Z-5 has macroporous and mesoporous structure in it [30]. In Fig. 7g, the curve become III-type, and there is a hysteresis loop in the middle section, which indicats that the sample Z-6 has weak interaction and mesoporous structure in it [30]. By the image of pore size distribution of samples in Fig. 7a–e, it can be found that inhomogeneous mesoporous pore sizes existed, and the average pore sizes obtained from the adsorption isotherm were about 3–4 nm and enlarged as the ratio of rGO increased. In Fig. 7f, macropore existed apparently and the average pore size was about 12 nm. But as the ratio of rGO further increased to 10 %, the average pore size decreased to 3–4 nm in Fig. 7g. According to the calculation of test software, it was found that the BET specific surface area of ZnO–rGO samples (Z-0.5, Z-1, Z-2, Z-4, Z-5 and Z-10) was 21.739, 25.166, 31.398, 51.564, 52.578 and 14.142 m^2/g , which was much higher than that of the ZnO sample (1.436 m^2/g). Apparently, the BET specific surface area of the sample Z-5 reached peak among all the samples, which may be attributed to its small grain

size (as shown in Fig. 6c) and large pore size (about 12 nm).

3.2 Measurements of gas sensing properties

The calculating method of concentration and injection volume for gas is described as following:

$$V_x = V \times C \times 10^{-6} \times [(273 + T_r)/(273 + T_c)]. \quad (1)$$

While for liquid, another equation is always used:

$$V_x = (V \times C \times M)/(22.4 \times d \times p) \times [(273 + T_r)/(273 + T_c)] \times 10^{-9}. \quad (2)$$

In Eq. (1) and (2), V_x and V represent the injection volume (mL) of detected gas and volume of the sealed chamber (18,000 mL), respectively. C is a variable quantity which shows concentration (ppm) of the detected gas. M , d and p are defined as molar mass, density (g/cm^3) and purity of detected gas. T_r and T_c are room temperature and sealed chamber temperature, respectively. For example, according to the calculation, about 1.5 mL hydrogen sulfide (10 %) makes the concentration reach 10 ppm in chamber. In the testing system, there are three parameters must be controlled: signal voltage, heating voltage and series resistance. The heating voltage is regulated to change operation temperature of the gas sensor, and the series resistance is altered to gain the proper signal voltage for the gas sensor [31].

The gas sensor devices were fixed in the testing circuit board, and tested at different concentrations (1, 2, 4, 5, 10, 20, 50 ppm) of hydrogen sulfide at 100, 160, 200, 240 and 300 $^\circ\text{C}$ respectively. Sensitivity is defined as R_a/R_g , R_a is the resistance of gas sensor in the air, R_g is the resistance of gas sensor in the tested gas. The response or recovery time is defined as the time taken for the change of signal voltage of sensor reach 90 % of its total changed value as shown in Fig. 10.

As shown in Fig. 8, when hydrogen sulfide concentration is in the range of 1–20 ppm, sensitivity response characteristic curves are almost linear. The sensitivity increased rapidly as the concentration increasing but slowly after the concentration was higher than 20 ppm. Apparently, the sample ZnO–rGO (5 wt%) has the highest gas response, which may be attributed to the proper introduction of graphene. But too much rGO doping may change the crystal structure of ZnO, which apparently had an impact on its gas sensing properties. So response to hydrogen sulfide of the sample ZnO–rGO (10 wt%) decreased obviously.

To find the best working temperature, sensitivity of all the samples to hydrogen sulfide were measured with the range of temperature from 100 to 300 $^\circ\text{C}$, as shown in

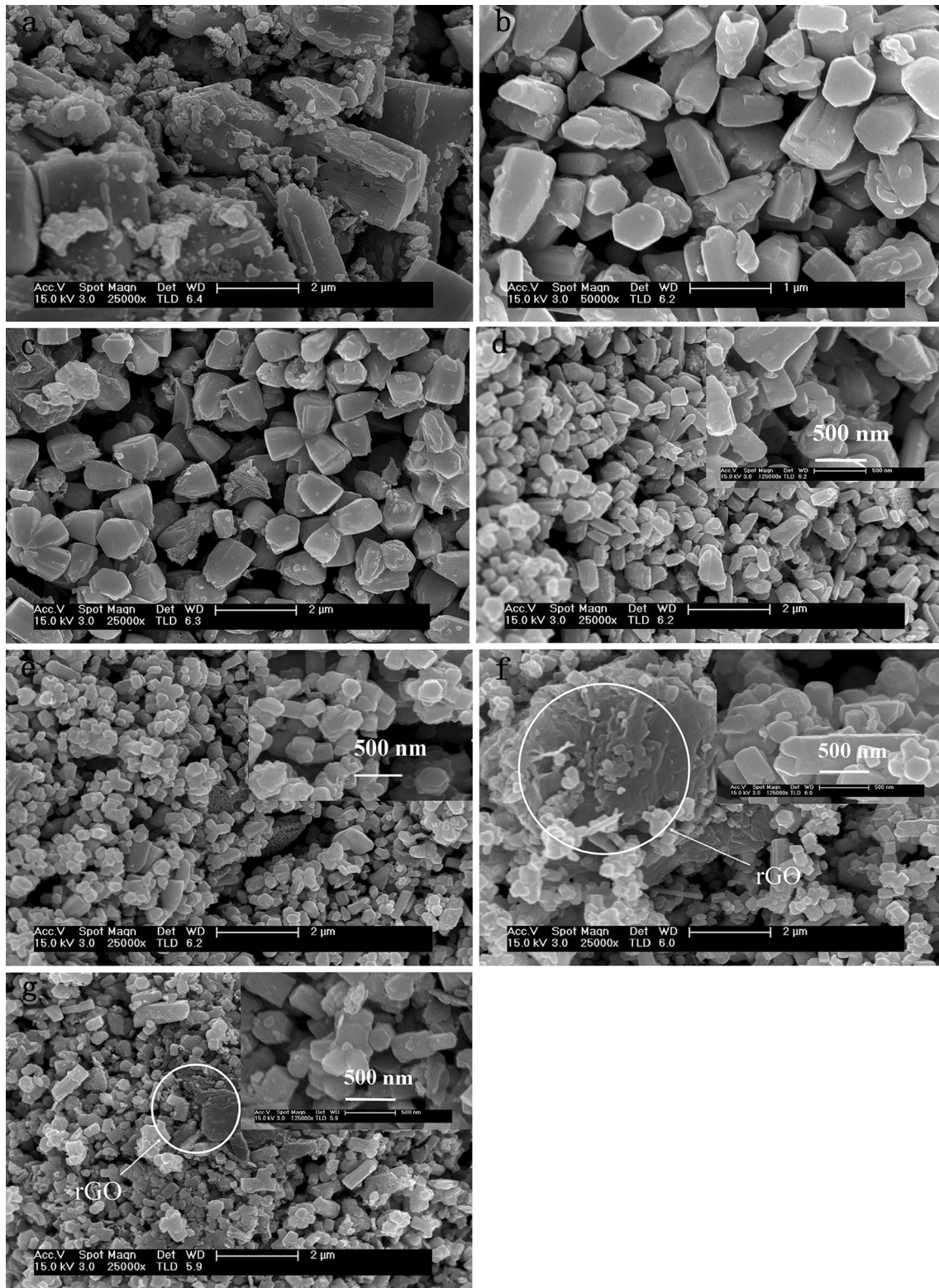


Fig. 6 FE-SEM images of surface of gas sensing layers by **a** Z-0, **b** Z-0.5, **c** Z-1, **d** Z-2, **e** Z-4, **f** Z-5, **g** Z-10

Fig. 9. Apparently, response of all the samples reach peak at 160 °C, and the introduction of rGO leads to an increase in response to hydrogen sulfide, the sample ZnO-rGO

(5 wt%) has the highest gas response. There are two types of gas adsorption in the surface of ZnO-rGO. Chemical adsorption and physical adsorption were happened on the

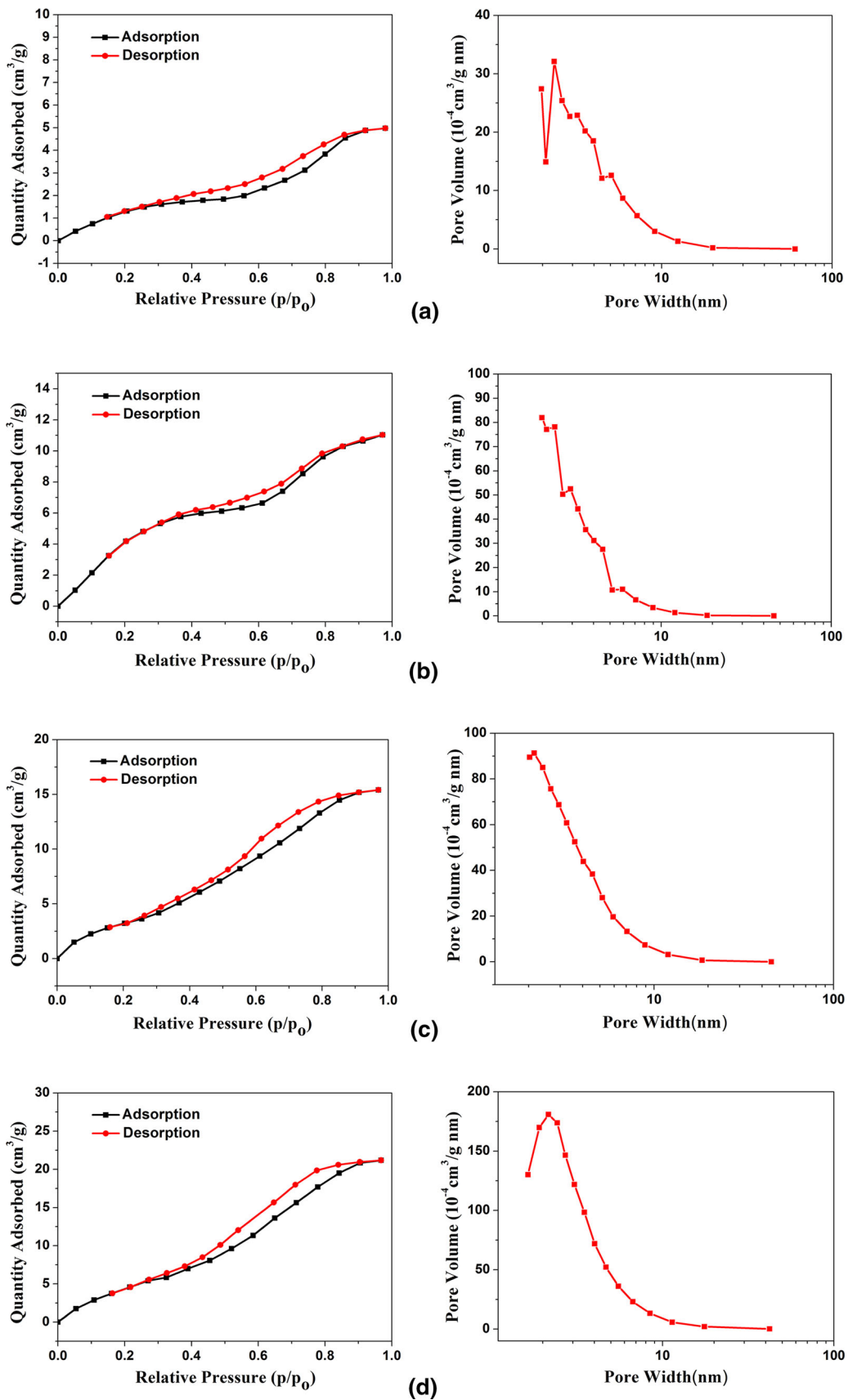


Fig. 7 N_2 adsorption–desorption curves of **a** Z-0, **b** Z-0.5, **c** Z-1, **d** Z-2, **e** Z-4, **f** Z-5, **g** Z-10

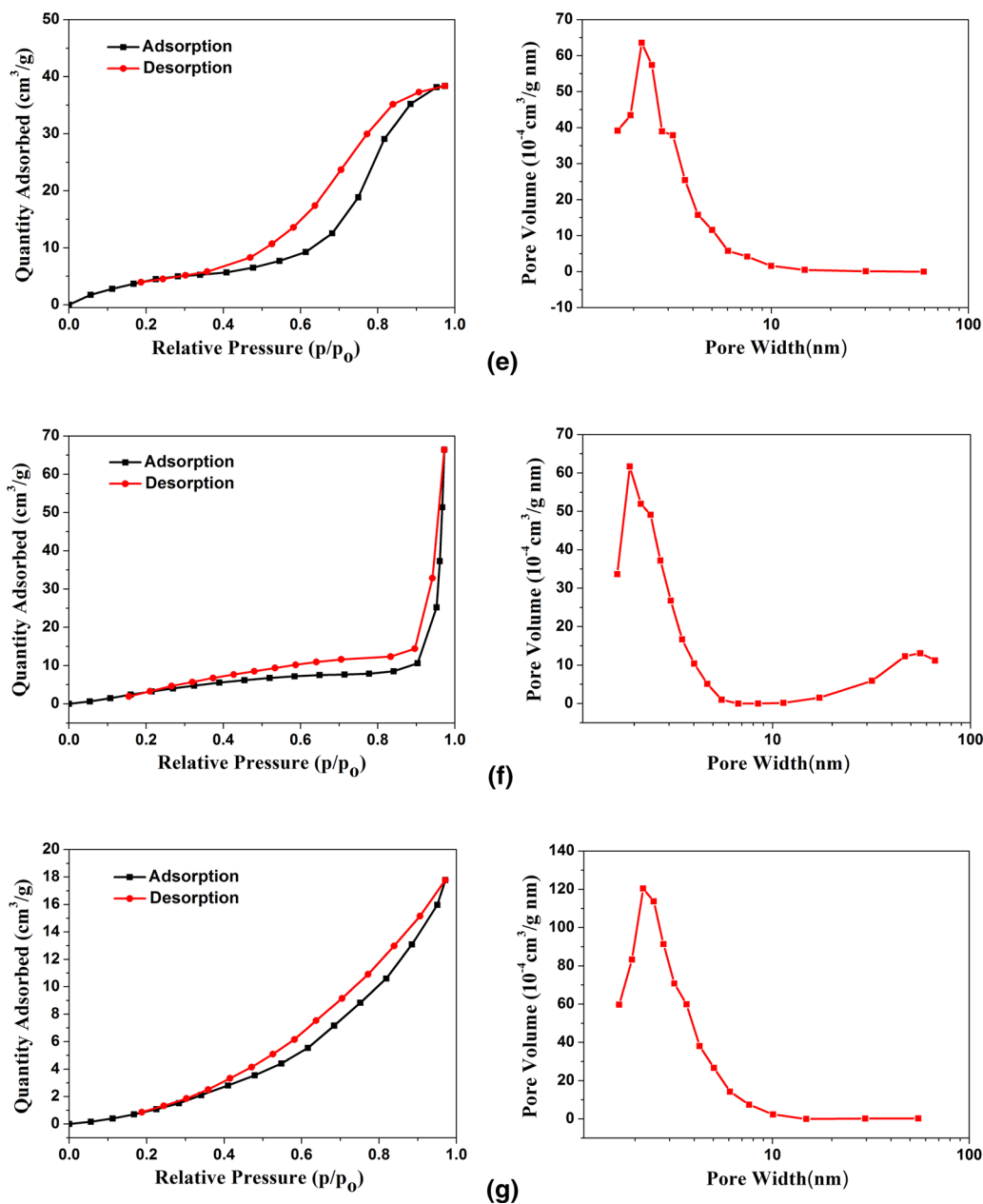


Fig. 7 continued

surface of ZnO and RGO, respectively. The physical adsorption can occur at low temperature, but at high temperatures, molecular vibrates at high speed, and slides on the surface of rGO, so desorption occurs. The chemical absorption depends on chemical bonds of gas molecules breaking, so it is difficult to occur at low temperature. In the range of 100°–160°, the physical adsorption plays a leading role, and because the temperature is low, the adsorption effect is almost not affected. With the increasing of temperature, chemical adsorption is increasing, so the gas response increased capacity. In the range of 160°–

300°, chemical adsorption is increasing, while the physical adsorption is decreasing, but the increased chemical adsorption cannot compensate for the decreased physical adsorption, as a result, the response to gas decreased. It is known that Zinc oxide has relatively high resistance at low temperature, while graphene has excellent conductivity. So adding proper graphene to Zinc oxide crystal may enhance the conductivity at low temperature effectively and resulted in the increase of response to hydrogen sulfide.

Figure 10a showed the response and recovery curve of sample Z-5 at 240 °C. It can be tested that the response

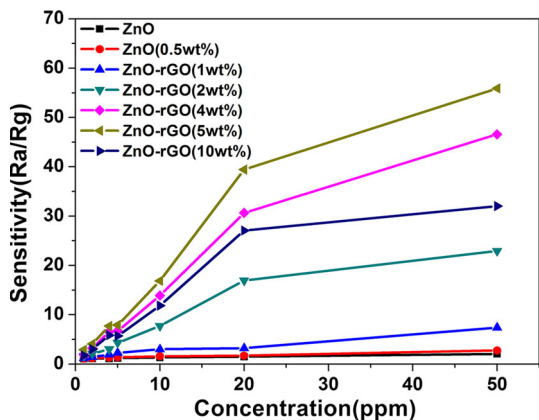


Fig. 8 Gas response versus concentration of hydrogen sulfide curve for pure ZnO and ZnO-rGO nanocomposites at 160° C

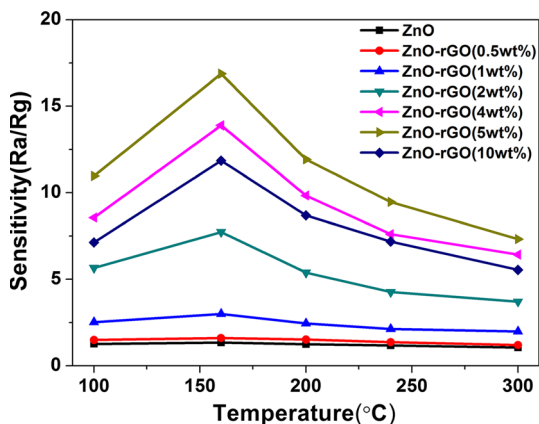


Fig. 9 Sensitivity of gas sensors fabricated by pure ZnO and ZnO-rGO nanocomposite to hydrogen sulfide (10 ppm)

time of the device is 35 s, and the recovery time of the device is 410 s. Response and recovery time of Z-5 at 100–300 °C to 10 ppm hydrogen sulfide were shown in Fig. 10b. As shown in the figure, response time was much less than recovery time, and both of them decreased as the temperature increased.

To obtain the selectivity of the samples, the gases including ethanol, methanol, acetone, formaldehyde, and ammonia were detected to compare with hydrogen sulfide. Figure 11 is the bar graph of the selectivity to hydrogen sulfide of gas sensor made by ZnO-rGO (5 wt%). It was seen that the gas sensor exhibited high response to hydrogen sulfide, which was much higher than other gases (concentration of all the gases is 10 ppm). It was known that the adsorption of the detected gases on the surface of ZnO-rGO depends on the nature of the gases, such as the polarity, molecular weight, and structure of the gas molecule. Hydrogen sulfide is polar molecule and has strong reducibility, thus easier to react with oxygen groups on the

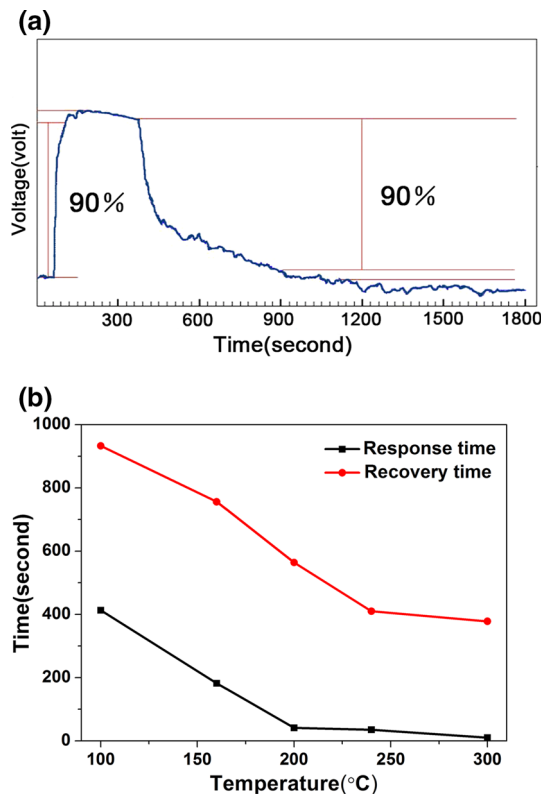


Fig. 10 a Response and recovery curve of ZnO-rGO (5 wt%) at 240 °C (10 ppm hydrogen sulfide). **b** Response and recovery time of ZnO-rGO (5 wt%) at 100–300 °C (10 ppm hydrogen sulfide)

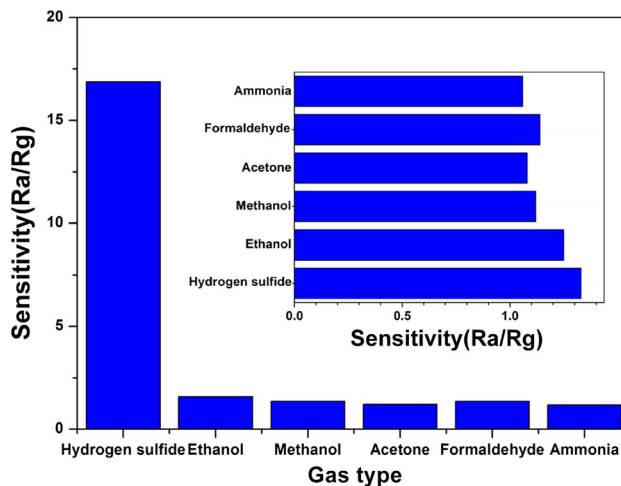


Fig. 11 Selectivity to hydrogen sulfide of gas sensor at 160° C made by Z-5 and Z-0

surface of gas sensors. The bar graph of the selectivity of Z-0 to hydrogen sulfide was shown in the inset image of Fig. 11. As we could see, response of device made by pure ZnO to all of the gases was not obvious at 160 °C, and the gas sensor had poor selectivity to hydrogen sulfide, which may be attributed to the large particle size and small BET

specific surface area of Z-0 synthesized by a hydrothermal method in alkaline condition.

4 Conclusions

In summary, a green and low-cost hydrothermal method assisted with Pluronic P123 triblock copolymer was used to prepare pure ZnO and ZnO–rGO nanocomposites, and the prepared materials were used to fabricate gas sensors. XRD results of prepared materials showed the formation of wurtzite ZnO. The D peak at 1366 cm^{-1} and G peak at 1577 cm^{-1} in Raman spectra of samples indicated the existence of rGO. According to the gas sensing test of fabricated devices, the best operation temperature was $160\text{ }^{\circ}\text{C}$. Mixing rGO apparently improved the sensitivity to hydrogen sulfide, and the best mixing rate was 5 wt%. The gas response to hydrogen sulfide of ZnO–rGO (5 wt%) reached 55.91 at $160\text{ }^{\circ}\text{C}$, which was about dozens of times higher than that of pure ZnO. The devices made by ZnO–rGO (5 wt%) exhibited excellent selectivities to hydrogen sulfide.

Acknowledgments The work was supported by National Basic Research Program of China (2012CB934300), Shanghai City Committee of Science and Technology (15520500200), National Nature Science Foundation of China (61006089), Innovation Program of Shanghai City (CX SJ-15-112) and Cooperation Fund of Shanghai Institute of Technical Physics.

References

1. A.R. Raju, C.N.R. Rao, *Sens. Actuators B* **3**, 305 (1991)
2. S. Roy, S. Basu, *Bull. Mater. Sci.* **25**, 513 (2002)
3. M. Hjiri, L. Mir, S.G. Leonardi, N. Donato, G. Neri, *Nanomaterials* **3**, 357 (2013)
4. A. Wei, L. Pan, W. Huang, *Mater. Sci. Eng. B* **176**, 1409 (2011)
5. Z.L. Wang, *J. Phys. Condens. Matter* **16**, 829 (2004)
6. J. Huang, Q. Wan, *Sensors* **9**, 9903 (2009)
7. A. Forleo, L. Francioso, S. Capone, P. Siciliano, P. Lommens, Z. Hens, *Sens. Actuators B* **146**, 111 (2010)
8. W. Guo, T. Liu, H. Zhang, R. Sun, Y. Chen, W. Zeng, Z.C. Wang, *Sens. Actuators B* **166**, 492 (2012)
9. S. Bai, T. Guo, D. Li, R. Luo, A. Chen, C.C. Liu, *Sens. Actuators B* **182**, 747 (2013)
10. M. Ramezani, S.M. Hosseinpour-Mashkani, A. Sobhani-Nasab, H.G. Estarki, *J. Mater. Sci. Mater. Electron.* **26**, 7588 (2015)
11. S.M. Hosseinpour-Mashkani, M. Ramezani, A. Sobhani-Nasab, M. Esmaeili-Zare, *J. Mater. Sci. Mater. Electron.* **26**, 6086 (2015)
12. M. Maddahfar, M. Ramezani, M. Sadeghi, *J. Mater. Sci. Mater. Electron.* **26**, 7745 (2015)
13. S.M. Hosseinpour-Mashkani, M. Maddahfar, A. Sobhani-Nasab, *J. Mater. Sci. Mater. Electron.* **27**, 474 (2016)
14. A. Sobhani-Nasab, M. Maddahfar, S.M. Hosseinpour-Mashkani, *J. Mol. Liq.* **216**, 1 (2016)
15. M. Seredych, T.J. Bandoz, *Chem. Eng. J.* **166**, 1032 (2011)
16. M. Seredych, O. Mabayoje, T.J. Bandoz, *Langmuir* **28**, 1337 (2012)
17. M. Seredych, O. Mabayoje, M.M. Kolésnik, V. Krstić, T.J. Bandoz, *J. Mater. Chem.* **22**, 7970 (2012)
18. C. Xu, X. Wang, J. Zhu, X. Yang, L. Lu, *J. Mater. Chem.* **18**, 5625 (2008)
19. I.V. Lightcap, T.H. Kosel, P.V. Kamat, *Nano Lett.* **10**, 577 (2010)
20. B. Adhikari, A. Biswas, A. Banerjee, *ACS Appl. Mater. Interfaces* **4**, 5472 (2012)
21. X. Zhou, X. Huang, X. Qi, S. Wu, C. Xue, F.Y.C. Boey, Q. Yan, P. Chen, H. Zhang, *J. Phys. Chem. C* **113**, 10842 (2009)
22. N. Song, H. Fan, H. Tian, *J. Mater. Sci.* **50**, 2229 (2015)
23. H.S. Song, M.G. Park, W. Ahn, S.N. Lim, K.B. Yi, E. Croiset, Z. Chen, S.C. Nam, *Chem. Eng. J.* **253**, 264 (2014)
24. A.S.M.I. Uddin, D.-T. Phan, G.-S. Chung, *Sens. Actuators B: Chem.* **207**, 362 (2015)
25. H.S. Song, M.G. Park, E. Croiset, Z. Chen, S.C. Nam, H. Ryu, K.B. Yi, *Appl. Surf. Sci.* **280**, 360 (2013)
26. X. Liu, J. Sun, X. Zhang, *Sens. Actuators B* **211**, 220 (2015)
27. S. Ameen, *Mater. Lett.* **136**, 379 (2014)
28. W.S. Hummers, R.E. Offeman, *J. Am. Chem. Soc.* **80**, 1339 (1958)
29. M. Guo, P. Diao, X. Wang, S. Cai, *J. Solid State Chem.* **178**, 3210 (2005)
30. W. Yang, Y. Xu, Y. Tang, C. Wang, Y. Hu, L. Huang, J. Liu, J. Luo, H. Guo, Y. Chen, W. Shi, Y. Wang, *J. Mater. Chem. A* **2**, 16030 (2014)
31. S. Luo, Y. Shen, Z. Wu, M. Cao, F. Gu, L. Wang, *Mater. Sci. Semicond. Process* **41**, 535 (2016)